minerals

MDPI

Article

Gem-Quality Green Cr-Bearing Andradite (var. Demantoid) from Dobšiná, Slovakia

Ján Štubňa [1,*], Peter Bačík [2], Jana Fridrichová [2], Radek Hanus [3], L'udmila Illášová [1], Stanislava Milovská [4], Radek Škoda [5], Tomáš Vaculovič [6] and Slavomír Čerňanský [7]

1. Gemmological Institute, Faculty of Natural Sciences, Constantine the Philosopher University in Nitra, Nábrežie mládeže 91, 949 74 Nitra, Slovakia; lillasova@ukf.sk
2. Department of Mineralogy and Petrology, Faculty of Natural Sciences, Comenius University in Bratislava, Ilkovičova 6, Mlynská dolina, 842 15 Bratislava, Slovakia; peter.bacik@uniba.sk (P.B.); fridrichova.jana2@gmail.com (J.F.)
3. Gemological Laboratory of e-gems.cz, 110 00 Prague, Czech Republic; kakt@centrum.cz
4. Earth Science Institute of the Slovak Academy of Sciences, Ďumbierska 1, 974 01 Banská Bystrica, Slovakia; milovska@savbb.sk
5. Department of Geological Sciences, Masaryk University, Kotlářská 2, 611 37 Brno, Czech Republic; rskoda@sci.muni.cz
6. Central European Institute of Technology, Masaryk University, Kamenice 5, 625 00 Brno, Czech Republic; tomas.vaculovic@ceitec.muni.cz
7. Department of Environmental Ecology, Faculty of Natural Sciences, Comenius University in Bratislava, Ilkovičova 6, Mlynská dolina, 842 15 Bratislava, Slovakia; slavomir.cernansky@uniba.sk

* Correspondence: janstubna@gmail.com

Received: 11 February 2019; Accepted: 4 March 2019; Published: 8 March 2019

check for updates

Abstract: Andradite, variety demantoid, is a rare gem mineral. We describe gem-quality garnet crystals from serpentinized harzburgites from Dobšiná, Slovakia which were faceted. Both the andradite samples were transparent, with a vitreous luster and a vivid green color. They were isotropic with refractive indices >1.81. The measured density ranged from 3.82 to 3.84 g·cm^{-3}. Andradite var. demantoid appeared red under Chelsea filter observation. Both samples contained fibrous crystalline inclusions with the typical "horsetail" arrangement. The studied garnet had a strong Fe^{3+} dominant andradite composition with 1.72–1.85 apfu Fe^{3+}, Cr^{3+} up to 0.15 apfu, Al^{3+} 0.03 to 0.04 apfu, V^{3+} up to 0.006 apfu substituted for Fe^{3+}, Mn^{2+} up to 0.002 apfu, and Mg up to 0.04 apfu substituted for Ca. Raman spectrum of garnet showed three spectral regions containing relatively strong bands: I—352–371 cm^{-1}, II—816–874 cm^{-1}, and III—493–516 cm^{-1}. The optical absorption spectrum as characterized by an intense band at 438 nm and two broad bands at 587 and 623 nm and last one at 861 nm, which were assigned to Fe^{3+} and Cr^{3+}. Transmission was observed in the ultraviolet spectral region (<390 nm), near the infrared region (700–800 nm), and around 530 nm in the green region of visible light, resulting in the garnet's green color.

Keywords: andradite; demantoid; gemstone; Raman spectroscopy; UV-Vis-NIR spectroscopy; X-ray fluorescence spectroscopy; gem-quality; garnet

1. Introduction

Slovakia has only a few occurrences which produce gem-quality minerals. For a long time in history, precious opal from Červenica-Dubník was the only mineral considered as a gemstone [1–7]. Only a few Slovak minerals, including quartz var. smoky quartz [8,9], sphalerite [8,10], pyrite [8], garnet var. almandine [8], hematite [8], and corundum var. sapphire [11–13] are suitable for faceting.

Andradite garnet, $Ca_3Fe_2Si_3O_{12}$, is a rock-forming mineral typically found in metamorphic rocks such as skarns and rodingites. The andradite crystal structure consists of alternating SiO_4 tetrahedra and FeO_6 octahedra, and Ca with eight-fold coordination. Several studies have been carried out on the crystal chemistry and the thermodynamic properties of andradite garnets [14–22]. Green to yellow-green andradite garnets, demantoid variety, represent one of the most appreciated and precious gemstones among the garnet-group minerals, due to their color, brilliance, and rarity [23–25]. Gem-quality andradite-garnet sources occur in Russia [26–29], Italy [30], Iran [31–33], Pakistan [25,34–37], Namibia [38–41], Madagascar [42–47], Afganistan [24], Switzerland [24], Canada [48], Mexico [49], and China [50].

Our goal is a mineralogical and crystal-chemical investigation of andradite var. demantoid from a serpentinite body in Dobšiná, Slovakia using various analytical methods.

Geological Setting

The serpentinized harzburgites from Dobšiná are part of the Jurassic mélange complex (Meliata Unit). This inner Western-Carpathian unit forms small nappes over the Central Western Carpathians [51]. The Meliata Ocean formed after the continental break up in the Anisian [52], probably as a back-arc basin, due to northward subduction of the Paleotethys oceanic crust beneath the Eurasian continent [53]. The back-arc basin (BAB) basalts and mid-ocean ridge basalts (MORB) were dominant in the Meliatic oceanic rift [54,55]. The association of eupelagic and deepwater pelagic sediments, basalts, dolerite dikes, gabbros, and serpentinized mantle peridotites found in the Meliata Unit clearly indicates an oceanic suite [56,57]. The geochemistry of the basalts reveals a normal mid-ocean ridge basalts (N-MORB) [(La/Sm) n = 0.6–0.9] composition [54,55]. Traces of obducted oceanic crust (blocks of basalts alternating with radiolarite layers) were also identified from deepwater sedimentary breccias with a radiolaritic matrix [58]. The Neotethyan Meliata Oceanic back-arc basin closed in the Late Jurassic, according to ^{40}Ar–^{39}Ar ages of white mica from the blueschists and U/Pb LA-ICP-MS age of metamorphic-metasomatic perovskite [59,60]. The Meliatic subduction–accretionary wedge [61] was incorporated into the Cretaceous orogenic wedge of the Central Western Carpathians [62] between 130 and 50 Ma dated by ^{40}Ar–^{39}Ar method on white micas [63] in the form of mostly small nappe-sheeted bodies, thrust over the Gemeric and Veporic units of the Central Western Carpathians [64,65]. The zircon (U-Th)/He data recorded three evolutionary stages: (i) cooling through the ~180 °C isotherm at 130–120 Ma related to the startling collapse of the accretionary wedge, following exhumation of the high-pressure slices in the Meliatic accretionary wedge; (ii) postponed exhumation and cooling of some fragments through the ~180 °C isotherm from 115 to 95 Ma due to ongoing collapse of this wedge; and (iii) cooling from 80 to 65 Ma, postdating the thrusting (~100–80 Ma) during the Late Cretaceous compression related to formation of the Central Western Carpathians orogenic wedge [66].

The Dobšiná quarry (48°49.622′ N, 20°21.977′ E) (Figure 1) is in a tectonic fragment of the Meliata tectonic unit overlying the Gemeric tectonic unit. The locality is famous for the occurrence of yellow-green Cr-rich andradite (demantoid) in serpentinite veins [67–69]. Andradite-bearing serpentinites are part of the Late Jurassic (to Early Cretaceous) serpentinite–blueschist mélange complex. The mélange complex contains talc–phengite–glaucophane schists, marbles, metaconglomerates, blueschists of magmatic and sedimentary origin, and serpentinites. All rocks form decimeter- to 100 m-sized fragments within the Late Jurassic very low-temperature greenschist-facies metasediments [70].

Partly-preserved magmatic structures of harzburgite consist of olivine (~70 vol. %), orthopyroxene (~25 vol. %), accessory spinel (~4 vol. %), and rare clinopyroxene (~1 vol. %). Magmatically corroded and partly dissolved porphyric orthopyroxene (±clinopyroxene) is enclosed in olivine matrix with spinel. Both pyroxenes show exsolution lamellae, of clinopyroxene in orthopyroxene, or orthopyroxene in clinopyroxene, respectively. Orthopyroxene often forms sigmoidally rotated porphyroclasts, including clinopyroxene exsolution lamellae. The serpentinized harzburgite contains serpentinite group minerals (antigorite replaced by chrysotile and lizardite), Cr-Fe spinel, perovskite, pyrophanite, Ti andradite, magnetite, and hematite, and rarely carbonates with talc, quartz, and characteristic relics of olivine, orthopyroxene, clinopyroxene, and spinel [70,71].

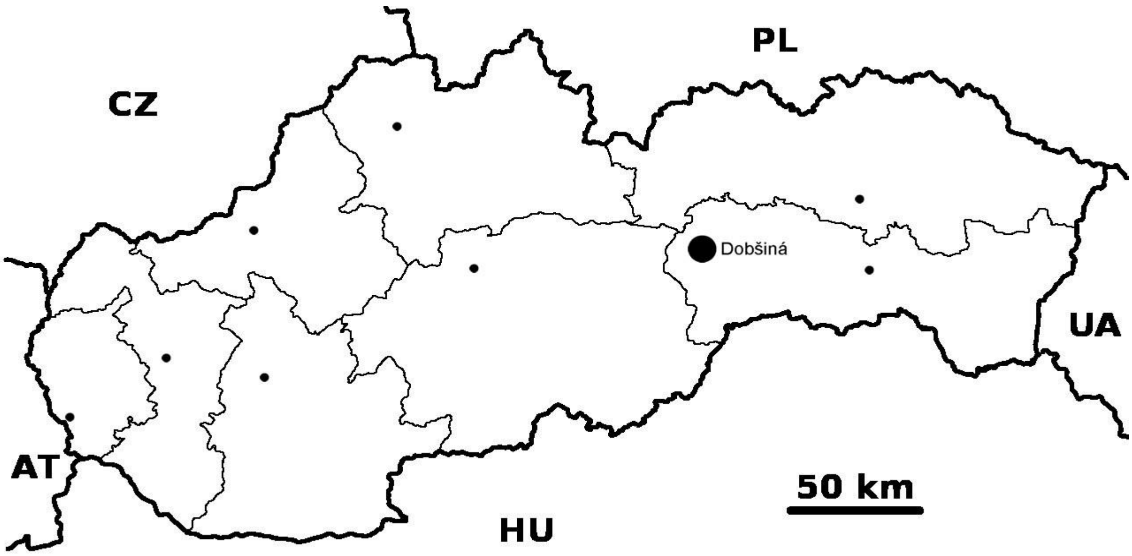

Figure 1. Locations of andradite var. demantoid source (small point—capital town of region) (CZ—Czech Republic, AT—Austria, HU—Hungary, UA—Ukraine, PL—Poland).

2. Materials and Methods

2.1. Sample Description

Two pieces of transparent andradite var. demantoid were separated from the host rock and faceted into round brilliant cuts with dimensions of 2.80 × 2.80 × 1.64 mm (0.11 carat) and 1.71 × 1.74 × 1.14 mm (0.025 carat) dimensions (Figure 2).

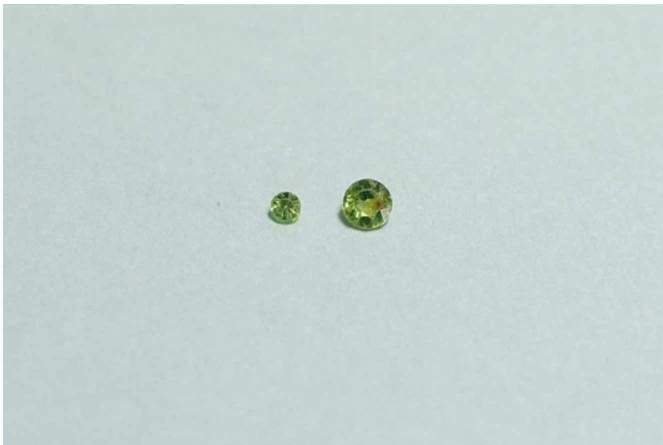

Figure 2. Andradite var. demantoid from Dobšiná, Slovakia (0.11 and 0.025 carat). Photo by J. Štubňa.

2.2. Analytical Methods

The faceted samples were examined by standard gemmological methods at the Gemmological Institute, Faculty of Natural Sciences, Constantine the Philosopher University in Nitra, to determine their optical properties (optical character and refractive indices), hydrostatic specific gravity, ultraviolet fluorescence, and microscopic features. The refractive indices were measured with a refractometer Kruss and Presidium Refractive Index Meter II. A Kern ABT 120-5DM with extension KERN ABT A01 hydrostatic balance was used to determine the density of the gemstones. The ultraviolet fluorescence was investigated with a short (254 nm) and long (366 nm) wavelength ultraviolet lamp. We used a Chelsea filter.

The chemical composition of andradite garnet was measured using a Cameca SX100 electron microprobe operated in wavelength-dispersion mode at the Masaryk University, Brno, Czech Republic, under the following conditions: accelerating voltage 15 kV, beam current 20 nA, and beam diameter 5 μm. The samples were analyzed with the following standards: fluorapatite (PKα), sanidine (SiKα, AlKα, KKα), titanite (TiKα), chromite (CrKα), vanadinite (VKα), YAG (YLα), almandine (FeKα), spessartine (MnKα), forsterite (Mg Kα), gahnite (ZnKα), wollastonite (CaKα), albite (NaKα), and topaz (FKα). Lower detection limits of the measured elements varied between 200–400 ppm except for Na (530–570 ppm), Fe (670–730 ppm), Zn (880–900 ppm), and Y (470–500 ppm). The measured content of Y, Mn, Zn, Na, and K was always below the detection limit. Analytical times were 15 to 40 s during measurement depending on the expected concentration of the element in the mineral phase. Major elements were measured using shorter times, whereas longer times were applied for elements with a low concentration. The andradite chemical formula was calculated based on 12 anions assuming all Fe as ferric.

Instrumentation for laser ablation inductively coupled plasma mass spectrometry (LA-ICP-MS) at the Department of Chemistry, Masaryk University, Brno, consists of a UP 213 laser ablation system (New Wave Research, Inc., Fremont, CA, USA) and Agilent 7500 CE ICP-MS spectrometer (Agilent Technologies, Santa Clara, CA, USA). A commercial Q-switched Nd-YAG laser ablation device worked at the 5th harmonic frequency corresponding to 213 nm wavelength. The ablation device was equipped with a programmable XYZ-stage to move the sample along a programmed trajectory during ablation. Target visual inspection and photographic documentation were achieved by the built-in microscope/CCD-camera system. A sample was enclosed in the SuperCell and was ablated by the laser beam, which was focused onto the sample surface through a quartz window. The ablation cell was flushed with a helium carrier gas which transported the laser-induced aerosol to the inductively coupled plasma (1 L·min^{-1}). Sample argon gas flow was admixed with the helium carrier gas flow after the laser ablation cell to 1.6 L·min^{-1} total gas flow. NIST SRM 610 silicate glass reference material was used to optimize the gas flow rates, the sampling depth, and MS electrostatic lens voltage in LA-ICP-MS conditions. This provided maximum signal-to-noise ratio and minimum oxide formation (ThO^+/Th^+ count ratio 0.2%, U^+/Th^+ counts ratio 1.1%). Laser ablation required a 100 μm laser spot diameter, 8 J·cm^{-2} laser fluence, and a 20 Hz repetition rate. The fixed sample position during laser ablation enabled 60 s hole-drilling duration for each spot. All element measurements were normalized on ^{28}Si in the investigated andradite. Analyses were gained from 10 spots in a line across the crystal.

Raman analyses were performed on the LabRAM-HR Evolution (Horiba Jobin-Yvon, Kyoto, Japan) spectrometer system with a Peltier cooled CCD detector and Olympus BX-41 microscope (Department of Geological Sciences, Masaryk University). Raman spectra excited by blue diode laser (473 nm) in the range of 50–4000 cm^{-1} were collected from each stone using 50× objectives. The acquisition time of 10 s per frame and 2 accumulations were used to improve the signal-to-noise ratio.

Optical absorption spectra of cut stones in the region (400–750 nm) were measured with the GL Gem SpectrometerTM at room temperature in the Gemmological Institute of Constantine the Philosopher University, Nitra. Both Raman and UV/Vis/NIR spectra were processed in Seasolve PeakFit 4.1.12 software. Raman and absorption bands were fitted by Lorentz function with the automatic background correction and Savitsky-Golay smoothing.

3. Results

Both the andradite samples were transparent, with a vitreous luster and a yellow-green color, which defines the andradite variety. They were all isotropic with refractive indices >1.81. The measured density ranged from 3.82 to 3.84 g·cm^{-3}, and the gemstones were inert in shortwave and longwave ultraviolet radiation. Andradite var. demantoid appeared red under Chelsea filter observation, which is typical for Cr-bearing gemstones. Both samples contained fibrous crystalline inclusions with the typical "horsetail" arrangement (Figure 3).

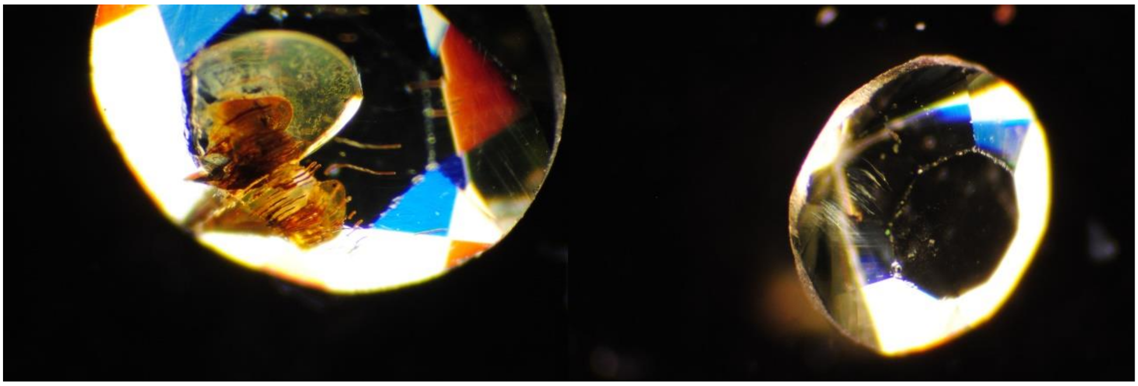

Figure 3. Fibrous crystalline inclusions of serpentine group minerals in andradite var. demantoid from Dobšiná, Slovakia. Photomicrograph by J. Štubňa; magnified 50×.

The studied garnet had a strongly Fe^{3+} dominant andradite composition with 1.72–1.85 apfu Fe^{3+} (Table 1 and Figure 4). Only Cr^{3+} (up to 0.15 apfu), Al^{3+} (0.03 to 0.04 apfu), and Mg (up to 0.04 apfu) substituted for Fe^{3+}. From the trace elements, Cr was the most abundant, along with moderate to minor concentrations (in relative decreasing order of abundance) of V, Ti, and Mn. The other trace elements measured (Sc, Ge, As, Y, and Gd) were near or below their respective detection limit (Table 2). There was no specific chemical zoning of crystal observed in major or trace elements.

Table 1. Electron microprobe analyses of demantoids, first provided in wt % of elements and then recalculated on the basis of 12 anions.

	1	**2**	**3**	**4**	**5**	**6**	**7**	**8**
P_2O_5	0.02	0.02	0.02	0.02	0.04	0.00	0.02	0.02
SiO_2	35.21	35.41	35.38	35.33	35.47	35.43	35.74	35.72
TiO_2	0.05	0.05	0.04	0.03	0.00	0.03	0.08	0.04
Al_2O_3	0.33	0.34	0.31	0.32	0.40	0.34	0.37	0.32
V_2O_3	0.09	0.07	0.07	0.08	0.07	0.09	0.06	0.05
Cr_2O_3	1.24	1.50	2.31	2.14	1.54	1.34	0.97	0.63
Fe_2O_3	29.15	29.15	27.69	28.34	28.64	28.82	29.16	29.65
MgO	0.20	0.23	0.20	0.17	0.34	0.23	0.20	0.21
CaO	33.88	33.80	33.74	33.72	33.85	33.85	33.74	33.65
F	0.08	0.11	0.09	0.11	0.09	0.08	0.09	0.10
O=F	−0.04	−0.05	−0.04	−0.06	−0.04	−0.04	−0.05	−0.05
Total	100.19	100.63	99.80	100.20	100.40	100.16	100.38	100.34
P^{5+}	0.002	0.001	0.001	0.001	0.003	0.000	0.001	0.001
Si^{4+}	2.975	2.977	2.993	2.981	2.984	2.990	3.003	3.004
F^-	0.021	0.028	0.023	0.030	0.023	0.022	0.024	0.026
Σ	2.997	3.006	3.018	3.012	3.010	3.012	3.029	3.031
Ti^{4+}	0.003	0.003	0.003	0.002	0.000	0.002	0.005	0.003
Al^{3+}	0.033	0.034	0.031	0.032	0.040	0.034	0.037	0.032
V^{3+}	0.006	0.005	0.005	0.006	0.005	0.006	0.004	0.003
Cr^{3+}	0.083	0.100	0.155	0.143	0.102	0.089	0.064	0.042
Fe^{3+}	1.845	1.837	1.757	1.793	1.806	1.823	1.840	1.873
Σ	1.969	1.979	1.950	1.975	1.953	1.954	1.950	1.952
Mg^{2+}	0.025	0.029	0.026	0.022	0.043	0.028	0.025	0.026
Ca^{2+}	3.067	3.044	3.059	3.049	3.052	3.060	3.037	3.032
Σ	3.092	3.073	3.084	3.071	3.095	3.089	3.063	3.058

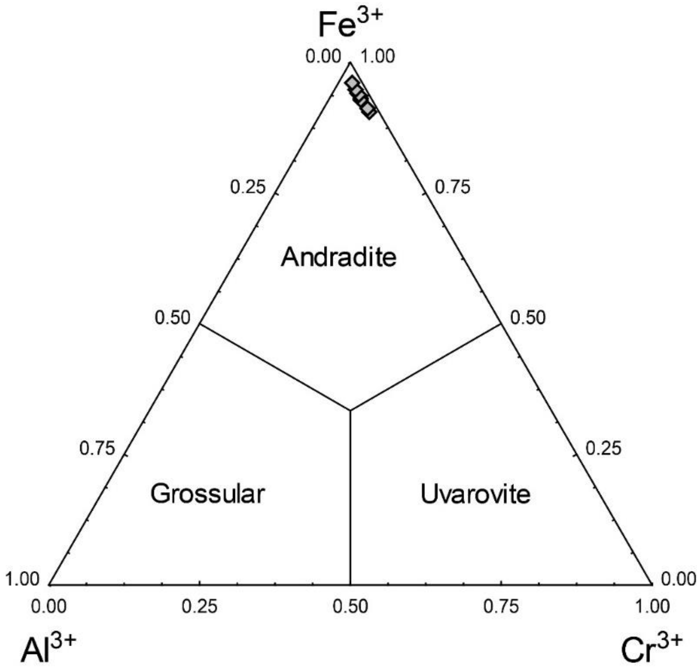

Figure 4. Ternary classification diagram of garnets.

Table 2. The trace-elements contents (in ppm) in demantoid from Dobšiná measured by laser ablation inductively coupled plasma mass spectrometry (LA-ICP-MS). (LOD—limit of detection).

	K	Sc	Ti	V^{51}	Cr^{53}	Mn	Ge^{72}	As^{75}	Y^{89}	Mo^{95}	Gd^{157}
Min	392	16	103	305	3814	103	4	11	2	0	0
Max	787	40	389	572	13331	224	13	22	5	1	2
Average	523	25	244	444	9199	143	9	16	3	1	1
LOD	48.7	2.1	11.4	0.7	9.2	7.8	3.8	9.1	0.1	0.1	0.1

From the calculated crystal-chemical formulae, it is obvious that *Z* site occupancy by Si is slightly lower than three. It could be filled to three by Al or Fe^{3+}, but their content is sufficient only to accommodate the *Y* site. Even after adding all possible octahedral cations, the *Y*-site sum is always slightly below two which, however, could result from the analytical error. However, the small deficiency at the *Z* site can be justified by the presence of F. The *X* site is almost uniformly occupied by Ca with a very small admixture of Mg.

Raman spectrum of garnet (Figure 5 and Table 3) showed three spectral regions containing relatively strong bands: I—352–371 cm^{-1}, II—816–874 cm^{-1}, III—493–516 cm^{-1}. The other bands exhibited relatively lower intensities. Measured bands were assigned to various molecular motions (Table 3): translation of SiO_4—T(SiO_4), rotation of SiO_4—R(SiO_4), translation of YO_6 (Y = Fe^{3+}, Cr^{3+})—T(M), symmetric band ν_2, asymmetric stretching frequency ν_3, asymmetric bending frequency ν_4 of SiO_4 group. Our spectrum is consistent with published andradite spectra [72], except the 343 cm^{-1} band, which is not present in published data. Only bands with similar Raman shift are in almandine and pyrope spectra associated with rotation of SiO_4 [72].

The optical absorption spectrum (Figure 6 and Table 4) is characterized by small absorption features below 370 nm, an intense band at 438 nm with shoulders at 470 and 488 nm, and two broad bands at 587 and 623 nm, and 861 nm with a shoulder at 964 nm. These spectral features were all assigned to Fe^{3+} and Cr^{3+}. Transmission was observed in the near the infrared region (700–800 nm), and around 530 nm in the green region of visible light resulting in the garnet's green color.

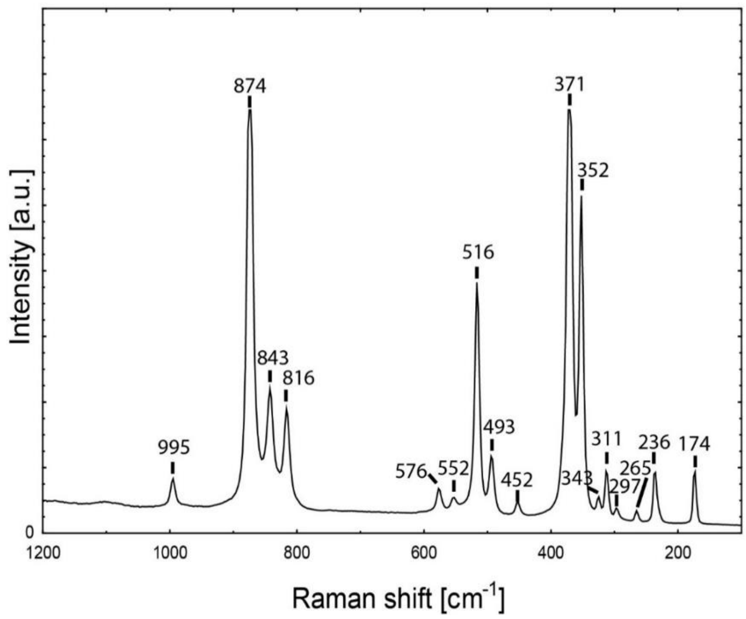

Figure 5. Raman spectrum of the andradite var. demantoid from Dobšiná, Slovakia.

Table 3. Raman shifts (cm^{-1}) of Raman-active bands in the studied sample. Assignment of band modes was made according to Reference [72].

Symmetry	Assignment	Demantoid Dobšiná	Andradite [72]
$T_{2g} + T_{1u}$	T(M)	174	173
$T_{2g} + T_{1u}$	T(M)	236	235
T_{2g}	$T(SiO_4)_{mix}$	265	264
E_g	$T(SiO_4)$	297	296
$T_{2g} + T_{1u}$	$T(SiO_4)$	311	311
?	?	343	-
E_g	ν_2	352	352
A_{1g}	$R(SiO_4)$	371	370
$T_{2g} + T_{1u}$	ν_2	452	452
E_g	ν_2	493	494
A_{1g}	ν_2	516	516
$T_{2g} + T_{1u}$	ν_4	552	553
E_g	ν_4	576	576
$T_{2g} + T_{1u}$	ν_3	816	816
$T_{2g} + T_{1u}$	ν_3	843	842
E_g	ν_3	874	874
$T_{2g} + T_{1u}$	ν_3	995	995

Table 4. The optical spectral bands (nm) in the studied sample. Assignment of bands was made according to Reference [22] and references therein.

Chromophores	Demantoid Dobšiná
Fe^{3+}	438
Fe^{3+}	470
Cr^{3+}	488
Fe^{3+}	587
Cr^{3+}	623
Fe^{3+}	861
Fe^{3+}	964

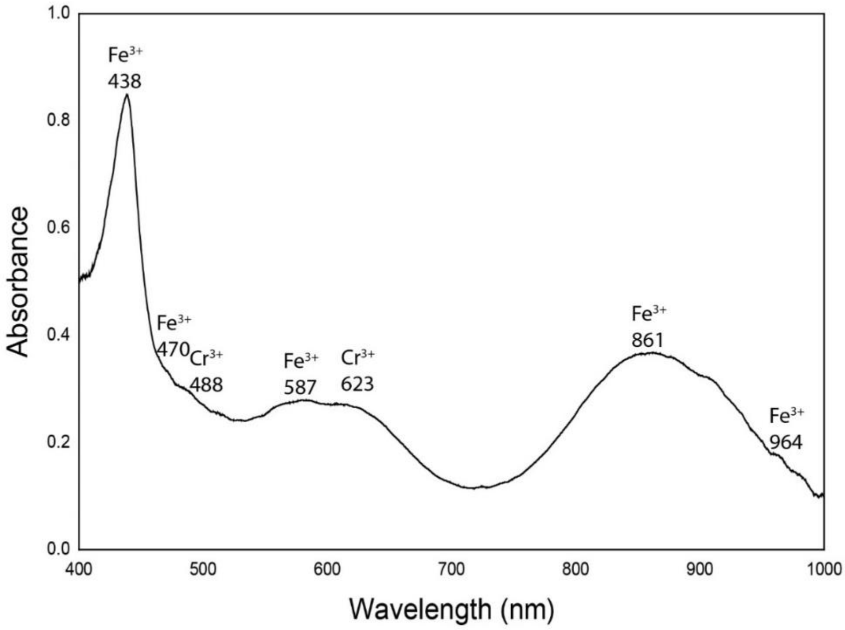

Figure 6. Optical absorption spectrum of the andradite var. demantoid from Dobšiná, Slovakia.

4. Discussion and Conclusions

Chromium-bearing garnets are relatively rare and are associated with specific geological environments and geochemical conditions. In the Western Carpathians, only a few occurrences have been described, including Pezinok–Rybníček [73], Čierna Lehota [74], and Dobšiná [67].

The garnet from Dobšiná occurs as the three following types [67]. The first type is present as relatively evenly dispersed minute grains in the rock. It originated preferentially at the expense of pseudomorphs after rhombic pyroxene. The garnet also forms lenticular or elongated layers 1 to 2 mm thick and several centimeters long. The second-type of garnet occurs as infilling of chrysotile veinlets. The veinlets' thickness is up to 3 mm. The third type of garnet forms monomineral fills in 0.3 to 3 mm-thick fissures. The garnet crystals display usually euhedral habit. However, only the third type of garnets are emerald-green color. All three garnet types occur in pale-colored, pale-green varieties of serpentinite.

Andradite color differences are caused by the variable Cr content. The studied garnet belongs to the third type which is generally enriched in Cr compared to the other two types. In some crystals of andradite, the determined value exceeded 6 wt % Cr_2O_3 [67], but the studied crystals only contain up to 2.3 wt % Cr_2O_3. However, this content is still significantly higher than in other demantoid occurrences around the world [21,30,47]. Moreover, demantoid from Dobšiná is enriched in V (up to 0.09 wt % V_2O_3 from EMPA, 305–572 ppm from LA-ICP-MS) compared to other localities with V usually below the detection limit of EMPA and below 270 ppm determined by LA-ICP-MS [21,30,47]. The As content between 10–22 ppm (although very close to the detection limit, were below detection limit on other localities [21]) and absence of REE (except very low Y), which are usually between 1–90 ppm [21] could also be a fingerprint feature for Dobšiná demantoid.

Raman mode analysis predicts the existence of 25 active Raman modes in all garnet species $3A_{1g}$, $8E_g$, and $14T_{2g}$. The vibrational spectra of garnet clearly possess two different groups of vibrational modes. The first group extends from 816 to 995 cm^{-1} in the Raman spectrum and possesses three strong bands and one weak one. In the garnet structure, these modes are commonly assigned to the ν_1 Si–O stretching motions within SiO_4 groups [72,75–78]. The second region extends from 174 to 576 cm^{-1} and possesses three strong and ten weak bands. The bands at 352, 452, 493, 516, 552, and 576 cm^{-1} are commonly assigned to the Si–O bending motions within SiO_4 groups [72]. The bands at 343 and

371 cm^{-1} can be assigned to rotation of the $[SiO_4]^{4-}$ tetrahedron $R[SiO_4]^{4-}$ [72]. The bands at 174, 236, 265, 297, and 311 cm^{-1} can be assigned to translation modes of the tetrahedra and octahedra [72].

The optical absorption spectra of studied garnet revealed a few absorption and transmission regions. The absorption feature at 438 nm and its shoulders are attributed to octahedral Fe^{3+}, although a further contribution from Cr^{3+} cannot be excluded [22,50,75,79–82], but this was not very significant due to the low Cr content. The weak absorption band at 488 nm is related to Fe^{3+} [30,47]. Two bands at 587 and 623 nm belong to octahedral Fe^{3+} and Cr^{3+}, respectively [22,50,75,79–82]. Presumed contribution of Cr^{3+} to the band at 438 nm can be assigned, according to the Tanabe–Sugano diagram [83–85], to the dominant $^4A_{2g} \rightarrow {}^4T_{2g}$ transition in Cr^{3+}. The second $^4A_{2g} \rightarrow {}^4T_{1g}$ transition in Cr^{3+} was at 623 nm but was overlapping with the Fe^{3+} absorption band at 587 nm. Moreover, a broad band at about 861 nm was due to octahedral Fe^{3+} [22,50,75,79–82].

Author Contributions: Concept of study, J.Š., R.H., J.F., and P.B.; methodology, J.Š., R.H., J.F., P.B, S.M., R.Š., T.V.; formal analysis, S.M., R.Š., T.V., and P.B.; formal investigation, J.Š., L'.I., J.F., and P.B.; compilation and writing of the manuscript, J.Š., J.F., and P.B.; review and editing of manuscript, J.Š., L'.I., J.F., S.Č., and P.B.

Funding: This present research was supported by the Ministry of Education of Slovak Republic grant agency under the contracts KEGA 062UKF-4/2016, VEGA-1/0079/15, VEGA-1/0499/16 and VEGA-1/0151/19.

Conflicts of Interest: The authors declare no conflict of interest.

References

1. Kaličiak, M.; Ďud'a, R.; Burda, P.; Kaličiaková, E. Structural geological characteristics of the Dubník opal deposits. *Zborník Vychodoslovenského Múzea v Košiciach* **1976**, *17*, 7–22.
2. Rondeau, B.; Fritsch, E.; Guiraud, M.; Renac, C. Opals from Slovakia ("Hungarian" opals): A re-assessment of the conditions of formation. *Eur. J. Mineral.* **2004**, *16*, 789–799. [CrossRef]
3. Gaillou, E.; Fritsch, E.; Aguilar-Reyes, B.; Rondeau, B.; Post, J.; Barreau, A.; Ostroumov, M. Common gem opal: An investigation of micro- to nano-structure. *Am. Mineral.* **2008**, *93*, 1865–1873. [CrossRef]
4. Gaillou, E.; Delaunay, A.; Rondeau, B.; Bouhnik-le-Coz, M.; Fritsch, E.; Cornen, G.; Monnier, C. The geochemistry of gem opals as evidence of their origin. *Ore Geol. Rev.* **2008**, *34*, 113–126. [CrossRef]
5. Kiefert, L.; Karampelas, S. Use of the Raman spectrometer in gemmological laboratories: Review. *Spectrochim. Acta-Part A Mol. Biomol. Spectrosc.* **2011**, *80*, 119–124. [CrossRef] [PubMed]
6. Caucia, F.; Marinoni, L.; Leone, A.; Adamo, I. Investigation on the gemological, physical and compositional properties of some opals from Slovakia ("Hungarian" opals). *Periodico di Mineralogia* **2013**, *82*, 251–261.
7. Caucia, F.; Ghisoli, C.; Marinoni, L.; Bordoni, V. Opal, a beautiful gem between myth and reality. *Neues Jahrbuch fur Mineralogie Abhandlungen* **2013**, *190*, 1–9. [CrossRef]
8. Ďud'a, R. Gemmological and genetic classification of precious and trim stones of Slovakia. *Mineral. Slovaca* **1987**, *19*, 353–362. (In Slovakian)
9. Fridrichová, J.; Bačík, P.; Illášová, L'.; Kozáková, P.; Škoda, R.; Pulišová, Z.; Fiala, A. Raman and optical spectroscopic investigation of gem-quality smoky quartz crystals. *Vib. Spectrosc.* **2016**, *85*, 71–78. [CrossRef]
10. Fridrichová, J.; Bačík, P.; Malíčková, I.; Illášová, L'.; Pulišová, Z. Optical-spectroscopic study of gem sphalerite from Banská Štiavnica and Hodruša-Hámre. *Esemestník* **2017**, *6*, 13–15. (In Slovakian)
11. Uher, P.; Sabol, M.; Konečný, P.; Gregáňová, M.; Táborský, Z.; Puškelová, L'. Sapphire from Hajnáčka Cérová Highland, southern Slovakia. *Slovak Geol. Mag.* **1999**, *5*, 273–280.
12. Uher, P.; Sabol, M.; Konečný, P.; Gregáňová, M.; Táborský, Z.; Puškelová, L'. Zafír vo výplni vrchnopliocénneho maaru pri Hajnáčke. *Miner. Slovaca* **2001**, *33*, 307–308.
13. Uher, P.; Giuliani, G.; Szakáll, S.; Fallick, A.; Strunga, V.; Vaculovič, T.; Ozdín, D.; Gregáňová, M. Sapphires related to alkali basalts from the Cerová Highlands, Western Carpathians (southern Slovakia): Composition and origin. *Geol. Carpath.* **2012**, *63*, 71–82. [CrossRef]
14. Quareni, S.; De Pieri, R. La struttura dell'andradite. Atti. e Memorie dell'. *Accademia Patavina di Science Lettere ed Arti* **1966**, *78*, 151–170.
15. Novak, G.A.; Gibbs, G.V. The crystal chemistry of the silicate garnets. *Am. Mineral.* **1971**, *56*, 791–825.
16. Hazen, R.M.; Finger, L.W. High-pressure crystal chemistry of andradite and pyrope: Revised procedure for high-pressure diffraction experiments. *Am. Mineral.* **1989**, *74*, 352–359.

17. Lager, G.A.; Armbruster, T.; Rotella, F.J.; Rossman, G.R. OH substitution in garnets: X-ray and neutron diffraction, infrared, and geometric-modeling studies. *Am. Mineral.* **1989**, *74*, 840–851.
18. Armbruster, T.; Geiger, C.A. Andradite crystal chemistry, dynamic X-site disorder and structural strain in silicate garnets. *Eur. J. Mineral.* **1993**, *5*, 59–71. [CrossRef]
19. Armbruster, T.; Birrer, J.; Libowitzky, E.; Beran, A. Crystal chemistry of Ti-bearing andradites. *Eur. J. Mineral.* **1998**, *10*, 907–921. [CrossRef]
20. Pavese, A.; Diella, V.; Pischedda, V.; Merli, M.; Bocchio, R.; Mezouar, M. Pressure-temperature equation of state of andradite and grossular, by high-pressure and -temperature powder diffraction. *Phys. Chem. Miner.* **2001**, *28*, 242–248. [CrossRef]
21. Bocchio, R.; Adamo, I.; Diella, V. Trace-element profiles in gem-quality green andradite from classic localities. *Can. Mineral.* **2010**, *48*, 1205–1216. [CrossRef]
22. Adamo, I.; Gatta, G.D.; Rotiroti, N.; Diella, V.; Pavese, A. Green andradite stones: Gemmological and mineralogical characterisation. *Eur. J. Mineral.* **2011**, *23*, 91–100. [CrossRef]
23. Balčiūnaitė, I.; Kleišmantas, A.; Norkus, E. Chemical composition of rare garnets, their colours and gemmological characteristics. *Chemija* **2015**, *26*, 18–24.
24. O'Donoghue, M. *Gems*, 6th ed.; Butterworth-Heinemann: Oxford, UK, 2006; p. 936.
25. Adamo, I.; Bocchio, R.; Diella, V.; Caucia, F.; Schmetzer, K. Demantoid from Balochistan, Pakistan: Gemmological and Mineralogical Characterization. *J. Gemmol.* **2015**, *34*, 428–433. [CrossRef]
26. Phillips, W.R.; Talantsev, A.S. Russian demantoid, czar of the garnet family. *Gems Gemol.* **1996**, *32*, 100–111. [CrossRef]
27. Krzemnicki, M.S. Diopside needles as inclusions in demantoid garnet from Russia: A Raman microspectrometric study. *Gems Gemol.* **1999**, *35*, 192–195. [CrossRef]
28. Laurs, B.M. A new find of demantoid at a historic side in Kladovka, Russia. *Gems Gemol.* **2003**, *39*, 54–55.
29. Mayerson, W.M. Lab Notes: Large demantoid of exceptional color. *Gems Gemol.* **2006**, *42*, 261–262.
30. Adamo, I.; Bocchio, R.; Diella, V.; Pavese, A.; Vignola, P.; Prosperi, L.; Palanza, V. Demantoid from Val Malenco, Italy: Review and update. *Gems Gemol.* **2009**, *45*, 280–287. [CrossRef]
31. Douman, M.; Dirlam, D. Update on demantoid and cat´s-eye from Iran. *Gems Gemol.* **2004**, *40*, 67–68.
32. Du Toi, G.; Mayerson, W.; van Der Bogert, C.; Douman, M.; Befi, R.; Koivula, J.I.; Kiefert, L. Demantoid from Iran. *Gems Gemol.* **2006**, *42*, 131.
33. Karampelas, S.; Gaillou, E.; Fritsch, E.; Douman, M. Les grenats andradites-démantoïde d'Iran: Zonage de couleur et inclusions. *Rev. Gemmol.* **2007**, *160*, 14–20.
34. Fritz, E.A.; Laurs, B.M. Gem News International: Andradite from Balochistan, Pakistan. *Gems Gemol.* **2007**, *43*, 373.
35. Milisenda, C.C.; Henn, U.; Henn, J. Demantoide aus Pakistan. *Gemmol. Z. Dtsch. Gemmol. Ges.* **2001**, *50*, 51–56.
36. Quinn, E.P.; Laurs, B.M. Demantoid from northern Pakistan. *Gems Gemol.* **2005**, *41*, 176–177.
37. Palke, A.C.; Pardieu, V. Gem News International: Demantoid from Baluchistan Province in Pakistan. *Gems Gemol.* **2014**, *50*, 302–303.
38. Lind, T.; Henn, U.; Bank, H. New occurrence of demantoid in Namibia. *Aust. Gemmol.* **1998**, *20*, 75–79.
39. Cairncross, B.; Bahmann, U. The Erongo Mountains, Namibia. *Mineral. Rec.* **2006**, *37*, 361–470.
40. Koller, F.; Niedermayar, G.; Pintér, Z.; Syabó, C. The demantoid garnets of the Green Dragon Mine (Tubussi, Erongo region, Namibia). *Acta Mineral.-Petrogr.* **2012**, *7*, 72.
41. Kaiser, H.; Enzersdorf, M. Demantoid aus der Green Dragon Mine, Erongo Region, Namibia. *Gemmo News* **2012**, *32*, 5.
42. Danet, F. Gem News International: New discovery of demantoid from Ambanja, Madagascar. *Gems Gemol.* **2009**, *45*, 218–219.
43. Rondeau, B.; Mocquet, B.; Lulzac, Y.; Fritsch, E. Les nouveaux grenats démantoïde d'Ambanja, Province d'Antsiranana, Madagascar. *Le Règne Mineral* **2009**, *90*, 41–45.
44. Rondeau, B.; Fritsch, E.; Mocquet, B.; Lulyac, Y. Ambanja (Madagascar)—New source of gem demantoid garnet. *InColor* **2009**, *11*, 16–20.
45. Praszkier, T.; Gajowniczek, J. Demantoide aus Antetezambato auf Madagascar. *Miner. Welt* **2010**, *21*, 32–41.
46. Pezzotta, F. Andradite from Antetezambato, North Madagascar. *Mineral. Rec.* **2010**, *41*, 209–229.
47. Pezzotta, F.; Adamo, I.; Diella, V. Demantoid and topazolite from Antetezambato, northern Madagascar: Review and new data. *Gems Gemol.* **2011**, *47*, 2–14. [CrossRef]

48. Wilson, B.S. Coloured gemstones from Canada. *Rocks Miner.* **2009**, *85*, 24–43. [CrossRef]
49. Ostrooumov, M. Mexican demantoid from new deposits. *Gems Gemol.* **2015**, *51*, 450–452.
50. Guobin, L.; Xu, K.; Lin, Z. On the Genesis of Demantoid from Xinjiang, China. *Chin. J. Geochem.* **1986**, *5*, 381–390. [CrossRef]
51. Mock, R.; Sýkora, M.; Aubrecht, R.; Ožvoldová, L.; Kronome, B.; Reichwalder, P.; Jablonský, J. Petrology and stratigraphy of the Meliaticum near the Meliata and Jaklovce Villages, Slovakia. *Slovak Geol. Mag.* **1998**, *4*, 223–260.
52. Kozur, H. The Evolution of the Meliata-Hallstatt ocean and its significance for the early evolution of the Eastern Alps and Western Carpathians. *Palaeogeogr. Palaeoclimatol. Palaeoecol.* **1991**, *87*, 109–135. [CrossRef]
53. Stampfli, G.M. The Intra-Alpine terrain: A Paleotethyan remnant in the Alpine Variscides. *Eclogae Geol. Helv.* **1996**, *89*, 13–42.
54. Ivan, P. Relics of the Meliata Ocean crust: Geodynamic implications of mineralogical, petrological and geochemical proxies. *Geol. Carpath.* **2002**, *53*, 245–256.
55. Faryad, S.W.; Spišiak, J.; Horváth, P.; Hovorka, D.; Dianiška, I.; Józsa, S. Petrological and geochemical features of the Meliata mafic rocks from the sutured Triassic Oceanic Basin, Western Carpathians. *Ofioliti* **2005**, *30*, 27–35.
56. Kozur, H.; Mock, R. New paleogeographic and tectonic interpretations in the Slovakian Carpathians and their implications for correlations with the Eastern Alps and other parts of the Western Tethys, Part II: Inner Western Carpathians. *Miner. Slovaca* **1997**, *29*, 164–209.
57. Kozur, H.; Mock, R. Erster Nachweis von Jura der Meliata-Einheit der südlichen Westkarpaten. *Geologisch-Paläontologische Mitteilungen Innsbruck* **1985**, *13*, 223–238.
58. Putiš, M.; Radvanec, M.; Hain, M.; Koller, F.; Koppa, M.; Snárska, B. 3-D analysis of perovskite in serpentinite (Dobšiná quarry) by X-ray micro-tomography. In *Proceedings of the Petros Symposium*; Ondrejka, M., Šarinová, K., Eds.; Univerzita Komenského: Bratislava, Slovakia, 2011; pp. 33–37.
59. Dallmeyer, R.D.; Neubauer, F.; Handler, R.; Fritz, H.; Müller, W.; Pana, D.; Putiš, M. Tectonothermal evolution of the internal Alps and Carpathians: $^{40}Ar/^{39}Ar$ mineral and whole rock data. *Eclogae Geol. Helv.* **1996**, *89*, 203–277.
60. Putiš, M.; Yang, Y.-H.; Koppa, M.; Dyda, M.; Šmál, P. U/Pb LA-ICP-MS age of metamorphic-metasomatic perovskite from serpentinized harzburgite in the Meliata Unit at Dobšiná, Slovakia: Time constraint of fluid-rock interaction in an accretionary wedge. *Acta Geol. Slovaca* **2015**, *7*, 63–71.
61. Faryad, S.W.; Henjes-Kunst, F. Petrological and K-Ar and 40Ar/39Ar age constraints for the tectonothermal evolution of the high-pressure Meliata unit, Western Carpathians (Slovakia). *Tectonophysics* **1997**, *280*, 141–156. [CrossRef]
62. Plašienka, D. Cretaceous tectonochronology of the central western Carpathians, Slovakia. *Geol. Carpath.* **1997**, *48*, 99–111.
63. Putiš, M.; Frank, W.; Plašienka, D.; Siman, P.; Sulák, M.; Biroň, A. Progradation of the Alpidic Central Western Carpathians orogenic wedge related to two subductions: Constrained by $^{40}Ar/^{39}Ar$ ages of white micas. *Geodin. Acta* **2009**, *22*, 31–56. [CrossRef]
64. Dal Piaz, G.; Martin, S.; Villa, I.M.; Gosso, G.; Marschalko, R. Late Jurassic blueschist facies pebbles from the Western Carpathians orogenic wedge and paleostructural implications for Western Tethys evolution. *Tectonics* **1995**, *14*, 874–885. [CrossRef]
65. Putiš, M.; Gawlick, H.J.; Frisch, W.; Sulák, M. Cretaceous transformation from passive to active continental margin in the Western Carpathians as indicated by the sedimentary record in the Infratatric Unit. *Int. J. Earth Sci.* **2008**, *97*, 799–819. [CrossRef]
66. Putiš, M.; Danišík, M.; Ružička, P.; Schmiedt, I. Constraining exhumation pathway in an accretionary wedge by (U-Th)/He thermochronology—Case study on Meliatic nappes in the Western Carpathians. *J. Geodyn.* **2014**, *81*, 80–90. [CrossRef]
67. Fediuková, E.; Hovorka, D.; Greguš, J. Compositional zoning of andradite from serpentinite at Dobšiná (West Carpathias). *Věst. Ústr. Úst. Geol.* **1976**, *51*, 339–345.
68. Hovorka, D.; Jaroš, J.; Kratochvíl, M.; Mock, R. The Mesozoic ophiolites of the Western Carpathians. *Krystalinikum* **1984**, *17*, 143–157.

69. Hovorka, D.; Ivan, P.; Jaroš, J.; Kratochvíl, M.; Reichwalder, P.; Rojkovič, I.; Spišiak, J.; Turanová, L. *Ultramafic rocks of the Western Carpathians, Czechoslovakia*; Geological Institute of Dionýz Štúr Publishers: Bratislava, Czechoslovakia, 1985; p. 258.
70. Putiš, M.; Koppa, M.; Snárska, B.; Koller, F.; Uher, P. The blueschist-associated perovskite-andradite-bearing serpentinized harzburgite from Dobšiná (the Meliata Unit), Slovakia. *J. Geosci.* **2012**, *57*, 221–240. [CrossRef]
71. Putiš, M.; Yang, Y.-H.; Vaculovič, T.; Koppa, M.; Li, X.-H.; Uher, P. Perovskite, reaction product of a harzburgite with Jurassic-Cretaceous accretionary wedge fluids (Western Carpathians, Slovakia): Evidence from the whole-rock and mineral trace element data. *Geol. Carpath.* **2016**, *67*, 133–146. [CrossRef]
72. Hofmeister, A.M.; Chopelas, A. Vibrational spectroscopy of end-member silicate garnets. *Phys. Chem. Miner.* **1991**, *17*, 503–526. [CrossRef]
73. Uher, P.; Kováčik, M.; Kubiš, M.; Shtukenberg, A.; Ozdín, D. Metamorphic vanadian-chromian silicate mineralization in carbon-rich amphibole schists from the Malé Karpaty Mountains, Western Carpathians, Slovakia. *Am. Mineral.* **2008**, *93*, 63–73. [CrossRef]
74. Bačík, P.; Uher, P.; Kozakova, P.; Števko, M.; Ozdín, D.; Vaculovič, T. Vanadian and chromian garnet- and epidote-supergroup minerals in metamorphosed Paleozoic black shales from Cierna Lehota, Strazovske vrchy Mountains, Slovakia: Crystal chemistry and evolution. *Mineral. Mag.* **2018**, *82*, 889–911. [CrossRef]
75. Peters, T. A water-bearing andradite from the Totalp serpentine (Davos, Switzerland). *Am. Mineral.* **1965**, *50*, 1482–1486.
76. Passaglia, E.; Rinaldi, R. Katoite, a new member of the $Ca_3Al_2(SiO_4)_3$-$Ca_3Al_2(OH)_{12}$ series and a new nomenclature for the hydrogrossular group of minerals. *Bulletin de la Société Française de Minéralogie et de Cristallographie* **1984**, *107*, 605–618. [CrossRef]
77. Galuskina, I.O.; Galuskin, E.V. Garnets of the hydrogrossular-“hydroandradite”-“hydroschorlomite” series. *Spec. Pap. Mineral. Soc. Pol.* **2003**, *22*, 54–57.
78. Galuskin, E. *Minerals of the Vesuvianite Group from the Achtarandite Rocks (Wiluy River, Yakutia)*; University of Silesia Publishing House: Katowice, Poland, 2005; p. 192.
79. Moore, R.K.; White, W.B. Electronic spectra of transition metal ions in silicate garnets. *Can. Mineral.* **1972**, *11*, 791–811.
80. Manning, P.G. Optical absorption spectra of Fe^{3+} in octahedral and tetrahedral sites in natural garnets. *Can. Mineral.* **1972**, *11*, 826–839.
81. Amthauer, G. Crystal chemistry and colour of chromium bearing garnets. *Neues Jahrbuch für Mineralogie Abhandlungen* **1976**, *126*, 158–186.
82. Stockton, C.M.; Manson, D.V. Gem andradite garnets. *Gems Gemol.* **1983**, *19*, 202–208. [CrossRef]
83. Tanabe, Y.; Sugano, S. On the absorption spectra of complex ions II. *J. Phys. Soc. Jpn.* **1954**, *9*, 766–779. [CrossRef]
84. Tanabe, Y.; Sugano, S. On the absorption spectra of complex ions I. *J. Phys. Soc. Jpn.* **1954**, *5*, 753–766. [CrossRef]
85. Tanabe, Y.; Sugano, S. On the absorption spectra of complex ions III. *J. Phys. Soc. Jpn.* **1956**, *11*, 864–877. [CrossRef]